Fluorinated Ether Based Electrolyte for High-Energy Lithium−Sulfur Batteries: Li+ Solvation Role Behind Reduced Polysulfide Solubility

Sara Drvarič Talian,[†,‡] Steffen Jeschke,[§] Alen Vizintin,[†] Klemen Pirnat,[†] Iztok Arčon,[⊥,¶] Giuliana Aquilanti,[#] Patrik Johansson,[§,∥] and Robert Dominko*,[†,‡,∥]

[†]Department of Materials Chemistry, National Institute of Chemistry, Hajdrihova 19, 1000 Ljubljana, Slovenia

[‡]Faculty of Chemistry and Chemical Technology University of Ljubljana, Večna pot 113, 1000 Ljubljana, Slovenia

[§]Department of Physics, Chalmers University of Technology, 412 96 Gothenburg, Sweden

[⊥]University of Nova Gorica, Vipavska 13, 5000 Nova Gorica, Slovenia

[¶]Institut Jožef Stefan, Jamova 39, 1000 Ljubljana, Slovenia

[#]Elettra-Sincrotrone Trieste S.C.p.A., s.s. 14 km 163.5, 34149 Basovizza Trieste, Italy

[∥]ALISTORE − European Research Institute, 33 rue Saint-Leu, Amiens 80039, France

S *Supporting Information*

ABSTRACT: By employing new electrolytes, the polysulfide shuttle phenomenon, one of the main problems of lithium−sulfur (Li−S) batteries, can be significantly reduced. Here we present excellent Coulombic efficiencies as well as adequate performance of high-energy Li−S cells by the use of a fluorinated ether (TFEE) based electrolyte at low electrolyte loading. The observed altered discharge profile was investigated both by electrochemical experiments and an especially tailored COSMO-RS computational approach, while the details of the discharge mechanism were elucidated by two *operando* techniques: XANES and UV−vis spectroscopy. A significant decrease of polysulfide solubility compared to tetraglyme is due to different Li+ solvation mode.
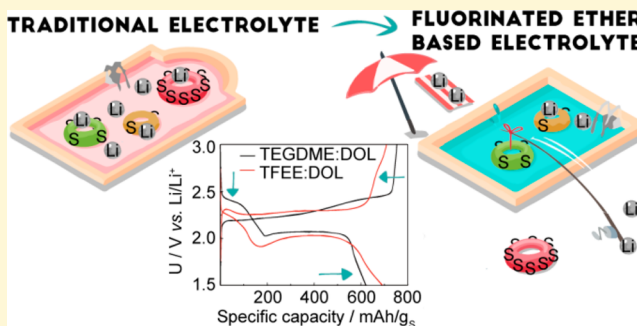
INTRODUCTION

Post Li-ion batteries are needed to accommodate the increasing world energy demand. Lithium−sulfur (Li−S) batteries are one of the leading technologies based on cheap starting materials and with a promise of high specific energy densities. Several fold increases in specific energy as compared to the Li-ion batteries[1] are predicted. However, there are still large problems to resolve. The discharge of a Li−S battery cell means reduction of elemental sulfur to lithium polysulfides and their dissolution into the electrolyte. The initially formed long-chain polysulfides are subsequently reduced in a series of reactions to short-chain polysulfides. The final product, Li_2S, is not soluble and precipitates on the cathode surface. The galvanostatic voltage profile typically features two plateaus: a high voltage plateau at about 2.4 V controlled by elemental sulfur and long-chain polysulfides reduction, and a low voltage plateau at 2.1 V representing the reduction of short-chain polysulfides to lithium sulfide.[2] Because of high polysulfide solubility in the electrolytes employed, several performance impeding effects take place, the most important being the polysulfide shuttle mechanism.[3,4]

Polysulfide dissolution is, however, essential for Li−S battery performance; therefore, efforts are focused on minimizing the polysulfide shuttling. Several approaches have been proposed in the literature; the most common concept is sulfur encapsulation to impair polysulfide dissolution and diffusion away from the cathode surface. Common matrices for this approach are porous carbon materials that range from carbon black materials,[5] carbon nanofibers[6] or nanotubes[7,8] to graphene[9] and reduced graphene oxide,[10] but metal oxides[11−13] have also been employed. Another approach is separator modifications: functionalization[14] or additional interlayers applied to both prevent polysulfide diffusion and protect the lithium metal anode.[15] A gel polymer electrolyte has the same functional principle.[16] A more novel way of reducing polysulfide shuttling involves the use of electrolytes that sparsely dissolve polysulfides such as acetonitrile[17,18] or fluorinated ethers.[19−21]

Here we utilized and investigated the use of an electrolyte composition with reduced polysulfide solubility based on the fluorinated ether 1,2-(1,1,2,2-tetrafluoroethoxy)ethane (TFEE) together with 1,3-dioxolane (DOL). Classic electrochemical characterization as well as *operando* analytical tools and

computational chemistry were all employed to study the mechanisms in detail. Furthermore, by using high loading sulfur cathodes and low electrolyte loadings, a high-energy Li−S battery cell was assembled and evaluated.

■ EXPERIMENTAL SECTION

Electrode and Electrolyte Preparation and Electrochemical Evaluation. A sulfur/carbon composite was prepared by mixing ENSACO 350G porous carbon (Imerys) and sulfur in a 1:2 weight ratio and heating the mixture in a sealed vessel under argon to 155 °C for 5 h. The composite with 66 wt % of sulfur was then mixed with Printex XE2 from Degussa and polyvinylidene fluoride (PVdF) in a mass ratio of 80:10:10 wt % in NMP. The slurry was cast on a carbon coated aluminum foil and dried at 50 °C overnight. The typical loading of sulfur for the PVdF electrodes was 1 mg S/cm^2. For the high-energy Li−S cells, the electrodes were prepared using the same electrode recipe but with an active mass loading of 4 mg S/cm^2.

As the sulfur K-edge XANES measurements performed in fluorescence detection mode require a lower ratio of sulfur in the cathode composite to diminish self-absorption effects,[22] a carbon−sulfur composite was prepared by mixing ENSACO 350G porous carbon (Imerys) and sulfur in 3:1 ratio. Electrodes were prepared by mixing Printex XE2 and polytetrafluoroethylene (PTFE) in a mass ratio 80:10:10 wt % in anhydrous isopropanol. Here the typical active mass loading was 0.5 mg S/cm^2. Teflon cathodes were pressed on a carbon coated aluminum mesh and used for the XAS experiments.

All electrolytes were prepared inside a glovebox from previously dried solvents and salt. The LiTFSI salt (Sigma-Aldrich, 99.95%) was dried overnight under vacuum at 140 °C, while the solvents were dried in a multistep process using molecular sieves, Al_2O_3, and distillation. TFEE (99.1%, Apollo scientific) was dried using molecular sieves (4A, ASGE, beads) for 5 days. The water content was measured by Karl Fischer titration (Mettler Toledo, C20) to be below 5 ppm. DOL (anhydrous, Sigma-Aldrich) was predried using molecular sieves (4A, ASGE, beads), dried with a K/Na alloy (wt. ratio 3/1) overnight by stirring at reflux temperature, and finally distilled at normal pressure, transferred into a flask (dried at 200 °C overnight) with good sealing, and stored. The final water content was below 2 ppm. TEGDME (99%, Acros, 174110010) was predried using molecular sieves (4A, ASGE, beads), distilled (5 mbar, 150 °C) to remove impurities and dried with a K/Na alloy (wt. ratio 3/1) overnight by stirring at 100 °C. Finally, it was again distilled (5 mbar, 150 °C), transferred into a flask (dried at 200 °C overnight) with good sealing, and stored. The final water content was below 5 ppm. All procedures were done inside the drybox to prevent any contamination by water. The electrolyte viscosities were determined at room temperature using a rotational rheometer Physoca MCR301 (Anton Paar) fitted with a cone-and-plate sensor system (CP50/2).

Pouch cells were assembled by wetting the cathode and Celgard 2400 separator with electrolytes of 1 M LiTFSI in different TFEE:DOL v:v ratios or 1 M LiTFSI in TEGDME:DOL 1:1 (v:v) and using metallic lithium (110 μm, FMC) as the anode. If not stated otherwise, 20 μL of electrolyte per mg of S was used. The cells were cycled at different C-rates by a sequence of: C/20 − C/10 − C/5 − C/2−1C (5 cycles each) − C/10 (75 cycles) in the potential range 1.5−3.0 V versus Li/Li+ using a Biologic VMP3 galvanostat/potentiostat.

When studying the effect of different solvent ratios (1:1, 1:2, and 2:1 v:v of TFEE and DOL), cells were prepared in the same way. For the construction of high energy Li−S battery cells, 6.5 μL (or less) of electrolyte per mg of S loading and high sulfur loading cathodes containing 4 mg of S/cm^2 were used. The cells were cycled at C/10 current density in the potential range of 1.5−3.0 V versus Li/Li+.

Computational Studies. The conductor-like screening model for real solvents (COSMO-RS) method[23−26] was applied for its ability to predict thermodynamic quantities and equilibria of fluids and liquid mixtures. The molecular structures of DOL, TEGDME, TFEE, 2H-tetrafluoroethyl 2,2,3,3-tetrafluoropropyl ether (TTE), and dimethoxyethane (DME) were built in the GUI of TmolX 4.2 and the initial QM

calculations were performed with the TURBOMOLE[27,28] V7.1 program package. All geometries were optimized using density functional theory (DFT) employing the BP86 functional[29,30] and the TZVP basis set[31] in gas phase and for a perfect conductor ($\varepsilon = \infty$). Additionally, single point calculations, BP86/TZVPD//BP86/TZVP, were performed to generate a fine grid cavity (FINE). The COSMO-RS calculations were performed with the COSMOthermX program[32] using the BP_TZVPD_FINE_C30_1701 parametrization at a temperature of 293.15 K. All COSMO-RS computations were performed for 1 M LiTFSI in TEGDME:DOL (1:1, v/v), TTE:DOL (1:1, v/v), and TFEE:DOL (1:1, v/v) using mole fractions based on the experimental densities for each electrolyte. For 1 M LiTFSI in DME:DOL (1:1, v/v), the mole fractions were calculated based on an estimated density. The TTE based electrolyte was added for comparison as it has already been experimentally reported for Li−S batteries.[33] An implicit solvation of Li+ was used since it has been proven to be a reliable approach for 1 M LiTFSI systems,[34] the molecular structure of sulfur was simplified to only consider the cyclo-S_8 allotrope[34] and the solid−liquid module was used to compute absolute solubilities. The polysulfide Li_2S_8 was described as a salt of two Li+ ions and one S_8^{2-} anion and its relative solubility was computed using the multiple-solvents module. The extended mixtures module was used to compute the intermolecular contact statistics and the chemical potentials of cyclo-S_8, Li+ and S_8^{2-}.

X-ray Absorption Spectroscopy (XAS). *Operando* sulfur K-edge XANES measurements were performed at the XAFS beamline of synchrotron Elettra (Basovizza, Trieste) in fluorescence-detection mode.[35] Experimental details are explained elsewhere[2,22] and summarized in the Supporting Information.

UV−vis and FTIR Spectroscopy. For the *operando* UV−vis spectroscopy study, pouch cell manufacture, assembly, and measurement procedures were carried out as described previously.[36,37] Because of the cell configuration, we used a higher electrolyte to S ratio: 60 μL/mg S. The cell was placed in a PerkinElmer Lambda 950 UV−vis spectrometer and discharged at a C/20 rate, with a cutoff voltage of 1.5 V versus Li/Li+, by using a Biologic SP-200 galvanostat/potentiostat. UV−vis spectra in the range 250−2000 nm were recorded every 30 min. Experimental details (and results) of the ATR-IR spectroscopy studies of the electrolytes are to be found in the Supporting Information.

■ RESULTS AND DISCUSSION

First, the electrochemical performance of TFEE based electrolytes was assessed and compared to a "traditional" Li−S battery electrolyte, 1 M LiTFSI in TEGDME:DOL 1:1 (v:v). Galvanostatic tests performed at different C-rates (Figure 1a) show that replacing TEGDME by TFEE improves the discharge capacity, but even more important, the Coulombic efficiency increases from about 82% to about 97% (at C/10 rate). Another remarkable difference is the altered voltage profiles (Figure 1b): the first discharge plateau is at 2.25 V for the TFEE based electrolyte, thus shifted by 150 mV (comparison by GITT experiments is shown in Figure S1), while the second discharge plateau is close to the thermodynamic potential for formation of Li_2S for both systems. Upon charging there is a similar shift of the higher voltage plateau to a lower potential for the TFEE containing electrolyte. Improved Coulombic efficiency and shifts of voltage plateaus are both connected with electrolyte polysulfide/sulfur solubility and it can be expected that different equilibria in the cell during the reduction and the oxidation processes influence the electrochemical processes. Thus, we propose that changes in the voltage profiles are thermodynamic and not kinetic in the origin.

To evaluate the influence of the two solvent components, TFEE and DOL, we studied cells using different solvent ratios (Figure 2a). High DOL content (1:2 ratio) leads to improved
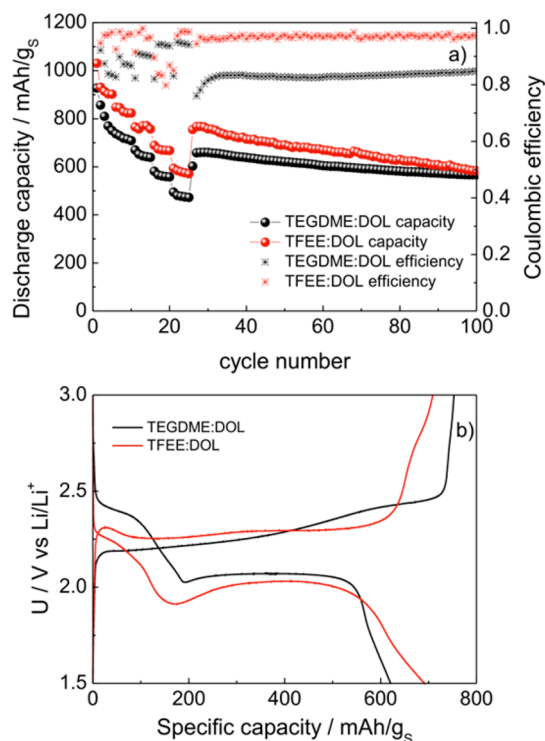
Figure 1. Electrochemical performance of cells with the fluorinated ether based electrolyte (TFEE) as compared to cells with a "traditional" electrolyte: (a) capacity and Coulombic efficiency at different C-rates and (b) voltage profiles for the 50th cycle (C/10). The solvent ratios for both the 1 M LiTFSI TEGDME:DOL and the 1 M LiTFSI TFEE:DOL electrolytes was 1:1 (v:v).
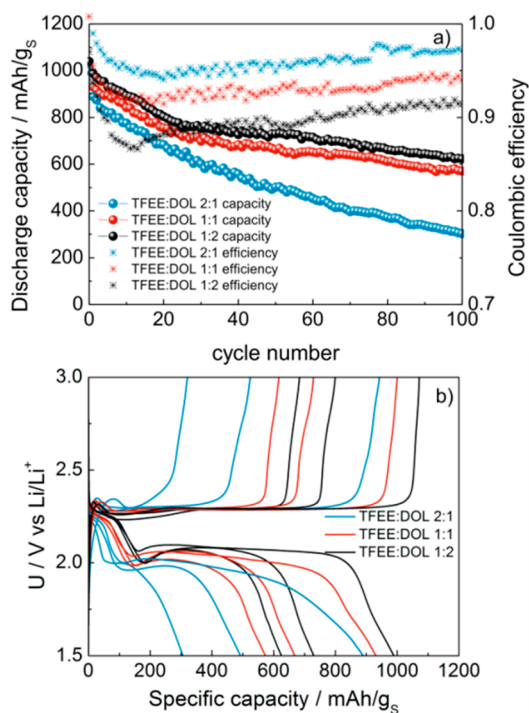

Figure 2. Cycling behavior at C/10 for 1 M LiTFSI containing electrolytes of different TFEE and DOL ratios, 1:2; 1:1; and 2:1 (v:v): (a) discharge capacity per g S in the cathode and Coulombic efficiency trend during 100 cycles, (b) charge and discharge voltage profiles for the 2nd, 50th, and 100th cycle.

capacity, but also poor cycling efficiencies, likely attributable to a large polysulfide solubility (and hence polysulfide shuttling). The trend is clear with intermediate specific capacities and cycling efficiencies for the 1:1 ratio and the TFEE:DOL 2:1 ratio electrolyte, as expected, showing the best Coulombic efficiency.

High TFEE content, however, increases the polarization of the cell (Figure 2b), observed as an increased difference between charge and discharge plateau. We attribute this to the increase in electrolyte viscosity from 0.0027 Pa s (1:2), via 0.0035 Pa s (1:1) to 0.0045 Pa s (2:1). Combined we can conclude that the best compromise for further evaluation, that is, high-energy Li−S battery cell experiments, is the 1 M LiTFSI in TFEE:DOL 1:1 (v:v) electrolyte.

Moving to the studies of the high-energy Li−S battery cell employing the optimized electrolyte above (1 M LiTFSI in TFEE:DOL 1:1) we obtained capacities over 1200 mAh/g_S and Coulombic efficiencies just below 97%, indeed without the use of any LiNO$_3$ additive (Figure 3). With an electrode loading of
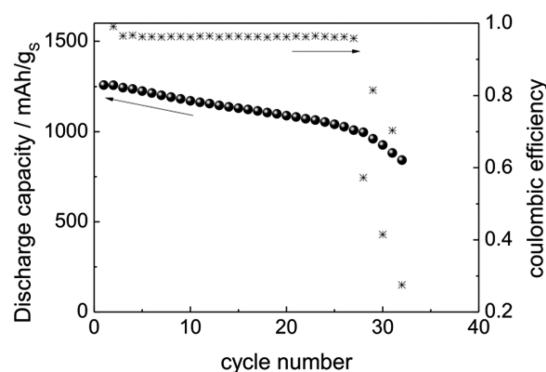

Figure 3. Discharge capacity per g S in the cathode and Coulombic efficiency for a cell with 6.5 μL of 1 M LiTFSI TFEE:DOL 1:1 electrolyte per mg S at C/10 rate. The electrode loading was 4 mg S/cm^2.

4 mg S/cm^2, the obtained areal capacity is close to 5 mAh/cm^2, basically fulfilling the requirements needed to enable a Li−S cell energy density above 500 Wh/kg. After about 25 cycles, grown lithium dendrites caused an internal short circuit, a consequence of the high areal capacity and a single layer of Celgard separator being employed. The stability of the Li metal anode was investigated by post mortem analysis (Figure S2) and impedance spectroscopy (Figure S3), which both support the claim that the anode causes the battery cell failure. Further decrease of electrolyte quantity is possible (Figure S4), but requires a complete redesign of the cathode porosity, and while a larger quantity increases the capacity, the Coulombic efficiency becomes poorer and a similar capacity fading can be observed (Figure S5). The cell with the larger amount of electrolyte could be cycled longer, supporting the hypothesis of cell failure being the Li metal anode consuming the electrolyte. While these preliminary results are quite encouraging for fluorinated ethers as Li−S battery electrolyte solvents, there are many open questions related to the exact mechanisms, for example, the substantial differences in the electrochemical curves.

The position of the high voltage plateau OCV is controlled by the dissolution of solid sulfur[38] and can arguably be proposed to be governed by the reaction of elemental sulfur with lithium to form the Li$_2$S$_8$ polysulfide. Hence, the Nernst

equation controlling the potential will be dependent on the activity of the polysulfide species and the sulfur dissolved in the electrolyte (eqs 1−3):

$$S_{8(diss)} + 2Li_{(s)} \rightleftarrows S_{8(diss)}^{2-} + 2Li_{(diss)}^{+} \tag{1}$$
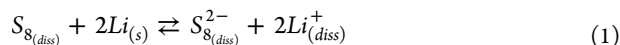
$$E = E^0 - \frac{RT}{zF} \ln \frac{a_{S_8^{2-}} \times a_{Li^+}^2}{a_{S_8}} \tag{2}$$

$$E \propto -\ln \frac{a_{S_8^{2-}}}{a_{S_8}} \tag{3}$$

By comparing eq 3 with the experimental relationship between the potentials in the two different types of electrolytes, "traditional" and fluorinated (eq 4), we deduce that the observed shift in potential for the high level plateau is due to the change in the ratio of activities of polysulfide ions and dissolved elemental sulfur (eqs 5−7):

$$E_{TEGDME} > E_{TFEE} \tag{4}$$

$$\left(\ln \frac{a_{S_8^{2-}}}{a_{S_8}} \right)_{TEGDME} < \left(\ln \frac{a_{S_8^{2-}}}{a_{S_8}} \right)_{TFEE} \tag{5}$$

$$\left(\frac{a_{S_8^{2-}}}{a_{S_8}} \right)_{TEGDME} < \left(\frac{a_{S_8^{2-}}}{a_{S_8}} \right)_{TFEE} \tag{6}$$

$$\frac{a_{S_8^{2-}TEGDME}}{a_{S_8^{2-}TFEE}} < \frac{a_{S_8 TEGDME}}{a_{S_8 TFEE}} \tag{7}$$

The above statement was further investigated using a stepwise COSMO-RS modeling approach to assess the solubility of elemental sulfur and polysulfides via their chemical potentials: (A) predict the absolute solubility of cyclo-S_8, (B) predict the relative solubility of Li_2S_8, (C) verify the validity of eq 7, (D) qualitatively address the differences between the TEGDME and the TFEE based electrolytes, and (E) analyze the chemical potential differences and the contact statistics for a further understanding of the Li_2S_8 solubility in different electrolytes.

The absolute cyclo-S_8 solubility (A) is calculated as a mole fraction x_i according to[39]

$$\ln(x_i) = \frac{\mu_i^{pure} - {}_{El}\mu_i - \Delta_{fus}G_i}{RT} \tag{8}$$

where μ_i^{pure} and ${}_{El}\mu_i$ are the chemical potentials of i as a pure compound and dissolved in the electrolyte, respectively, and $\Delta_{fus}G_i$ is its Gibbs energy of fusion. With a $\Delta_{fus}G$ of 2.9 kcal mol^{-1} for cyclo-S_8, absolute mole fraction solubilities of 1.0×10^{-4} (1−4 mM), 2.3×10^{-5} (0.1−1 mM), and 3.1×10^{-5} (0.1−1 mM) were calculated for the TEGDME, TTE, and TFEE based electrolytes, respectively. Thus, the solubility of sulfur is reduced by applying the fluorinated compounds.

The relative solubility is also calculated using eq 8, but when $\Delta_{fus}G$ is unknown, as for the polysulfide Li_2S_8 (B), it is set to 0 and thereby treats the compound as a supercooled liquid. In Figure 4, the calculated mole fraction solubilities are ranked using a logarithmic scale with the highest solubility set to 0 (for the TEGDME based electrolyte). Accordingly, the Li_2S_8 solubility is about four-times higher in the "traditional" TEGDME based electrolyte than in the DME based electrolyte and about 1000-times higher than in the fluoroether TTE or
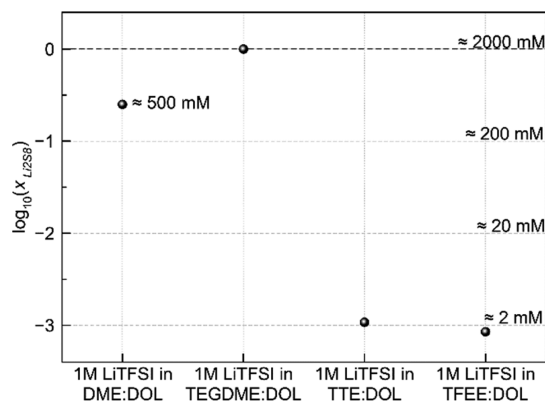

Figure 4. Computed relative solubilities from the COSMO-RS approach.

TFEE based electrolytes. The 1 M LiTFSI in DME:DOL (1:1, v/v) electrolyte with a reported absolute Li_2S_8 solubility of ~500 mM[40] has been added in Figure 4 to provide a rough estimate for the absolute Li_2S_8 solubility.

A quantitative verification of eq 7 (C) is made possible by considering the differences as a result of a liquid−liquid ion transfer process, which has already been investigated using COSMO-RS.[41] Hence, the transfer activity coefficient ${}_{A \to B}\gamma_i$ is introduced, which describes the difference of chemical potentials μ in standard states of a solute i in either electrolyte medium A and B and is therefore related to the Gibbs energy of transfer, ${}_{A \to B}G_i^0$, via[42]

$$\ln\left({}_{A \to B}\gamma_i\right) = \frac{\Delta_{A \to B}G_i^0}{RT} = \frac{{}_B\mu_i^0 - {}_A\mu_i^0}{RT} = \ln\left(\frac{a_{iA}}{a_{iB}}\right) \tag{9}$$

For A = TEGDME and B = TFEE (or TTE) based electrolytes and $i = S_8^{2-}$ or S_8, eq 7 is further simplified to

$${}_{TEGDME \to TFEE}\gamma_{S_8^{2-}} < {}_{TEGDME \to TFEE}\gamma_{S_8} \tag{10}$$

Since the absolute solubility of Li_2S_8 is unknown (see B), μ_i^0, ${}_{A \to B}G_i^0$ and ${}_{A \to B}\gamma_i$ have all been calculated for a few assumed mole fraction solubilities of 10^{-4}, 10^{-3}, 10^{-2}, and 10^{-1}, which correspond to solute concentrations of 1, 10, 100, and 1000 mM, respectively (Table 1). Hence, eq 10 is valid, indicating that the experimentally observed difference in the electrochemical potential indeed is a consequence of different solubilities of S_8 and Li_2S_8 in the TEGDME and TFEE based electrolytes.

The qualitative analysis of electrochemical potential difference for the formation of Li_2S_8 in the two electrolytes (D) start with a correlation with ${}_{A \to B}G_{Li_2S_8}^0$ via[41]

$$\Delta_{A \to B}E = -\Delta_{A \to B}G_{Li_2S_8}^0/zF \tag{11}$$

with[42]

$$\Delta_{A \to B}G_{Li_2S_8}^0 = 2 \times \Delta_{A \to B}G_{Li^+}^0 + \Delta_{A \to B}G_{S_8^{2-}}^0 \tag{12}$$

On the basis of the computed relative solubilities (Figure 4), the chemical potentials for Li^+ and S_8^{2-} at $x_{Li_2S_8} = 10^{-1}$ and $x_{Li_2S_8} = 10^{-4}$ were used for the "traditional" TEGDME based electrolyte and the fluoroether TTE or TFEE based electrolytes, respectively, to account for the different solubilities. With ${}_{TEGDME \to TTE}G_{Li_2S_8}^0 = 2.2$ kcal mol^{-1} and ${}_{TEGDME \to TFEE}G_{Li_2S_8}^0 = 2.3$ kcal mol^{-1}, potential differences of −47 and −50 mV were

Table 1. Computed Chemical Potentials $_E\mu_i$ for Different Electrolytes A and B at Different Mole Fractions x_i ($i = S_8$, $S_8{}^{2-}$, Li^+) and Transfer Activity Coefficients $_{A\to B}\gamma_i$ Calculated According to Eq 9[a]

	$x_{Li_2S_8}$				x_{S8}
	10^{-4}	10^{-3}	10^{-2}	10^{-1}	
	~1 mM	~10 mM	~100 mM	~1000 mM	
A: 1 M LiTFSI in TEGDME:DOL (1:1, v/v)					
$\mu_{S_8{}^{2-}}$	−6.6	−6.0	−5.0	5.1	
μ_{Li^+}	9.9	9.6	9.2	5.0	
μ_{TFSI}	1.0	1.2	1.6	6.5	
μ_{S_8}					−10.1
B: 1 M LiTFSI in TTE:DOL (1:1, v/v)					
$\mu_{S_8{}^{2-}}$	−7.8	−7.1	−5.7	4.9	
μ_{Li^+}	12.5	12.3	11.6	6.2	
μ_{TFSI}	1.9	2.1	2.5	6.7	
μ_{S_8}					−9.2
B: 1 M LiTFSI in TFEE:DOL (1:1, v/v)					
$\mu_{S_8{}^{2-}}$	−7.3	−6.7	−5.5	4.7	
μ_{Li^+}	12.4	12.1	11.5	6.3	
μ_{TFSI}	2.2	2.4	2.8	6.8	
μ_{S_8}					−9.4
$\Delta_{TEGDME\to TTE}G^0_{S_8{}^{2-}}$	−1.2	−1.1	−0.7	−0.2	0.9
$_{TEGDME\to TTE}\gamma_{S_8{}^{2-}}$	0.13	0.14	0.30	0.70	4.45
$\Delta_{TEGDME\to TFEE}G^0_{S_8{}^{2-}}$	−0.8	−0.7	−0.5	−0.3	0.7
$_{TEGDME\to TFEE}\gamma_{S_8{}^{2-}}$	0.27	0.29	0.45	0.56	3.29

[a]Transfer activity coefficients for S_8 $_{A\to B}\gamma_i$ were computed based on the calculated absolute solubilities (see A).

calculated, respectively, qualitatively consistent with the experimentally observed difference of −150 mV. In more detail on the origins of these macro-level observations in local interactions etc. (E), we start by the negative $\Delta_{A\to B}G^0_{S_8{}^{2-}}$ (Table 1), indicating that the polysulfide actually "prefers" the fluoroether based electrolytes over the traditional. Thus, from an energetic perspective, the driving force for the significant decrease in polysulfide solubility in the fluoroether based electrolytes is hence rather a worse stabilization of Li^+ ($_{A\to B}G_{Li^+}^0 \approx 2.5$ kcal mol^{-1}) and TFSI ($_{A\to B}G_{TFSI}^0 \approx 1.0$ kcal mol^{-1}). To further scrutinize the interaction on the molecular level, contact statistics for pairwise interactions[43] between $a = [S_8{}^{2-}$, Li^+, TFSI] and $b = [S_8{}^{2-}$, Li^+, TFSI, TEGDME/TFEE, DOL] in the TEGDME and TFEE based electrolytes were computed. The obtained contact probabilities, p_{ab}, were normalized by dividing by the initial mole fraction of the interacting compound b to allow the two electrolytes to be compared qualitatively:

$$N_{ab} = p_{ab}/x_b \tag{13}$$

From this three unique cases are distinguishable: $N_{ab} < 1$, less favorable contact ("repulsive" interaction), $N_{ab} > 1$, favorable contact ("attractive" interaction), $N_{ab} \approx 1$, neutral contact.

The formation of clusters such as $LiS_8{}^-$ and LiTFSI is highly favored in the TFEE based electrolyte (Table 2). The tendency of Li^+ to be in contact with the anions doubles from 4.7 and 1.3 in the TEGDME based electrolyte to 11.0 and 2.7 in TFEE based electrolyte for $S_8{}^{2-}$ and TFSI, respectively. Additionally, $S_8{}^{2-}$ shows a higher affinity toward the cation. Furthermore, TEGDME is highly likely to interact with the anions and Li^+, as

Table 2. Normalized Contact Probabilities N_{ab} for Ions in TEGDME and TFEE Based Electrolytes

	scrutinized compound a in:					
	1 M LiTFSI in TEGDME:DOL (1:1, v/v)			1 M LiTFSI in TFEE:DOL (1:1, v/v)		
interacting compound b	$S_8{}^{2-}$	Li^+	TFSI	$S_8{}^{2-}$	Li^+	TFSI
$S_8{}^{2-}$	0.9	4.7	1.3	0.8	11.0	1.0
ether	2.3	1.5	2.5	1.5	0.2	1.8
DOL	0.8	0.6	0.9	0.8	1.2	0.8
Li^+	0.6	0.0	0.2	1.4	0.0	0.4
TFSI	1.1	1.3	1.5	0.8	2.7	1.1

well-known for ethylene glycol derivatives. However, in TFEE the ether oxygen atoms are more shielded, limiting the contact with Li^+ significantly, whereas the interaction with the anions remains attractive. As a result, DOL becomes more important for the solvation of Li^+ for this electrolyte. In the Supporting Information, an FTIR spectroscopy based analysis of these interactions is outlined (Figures S6 and S7), but unfortunately severe band overlap makes it ambiguous.

The observed differences between the TFEE and TEGDME based electrolytes in terms of sulfur and polysulfide solubility may impact the reduction mechanism in the Li−S cells. Here we therefore employed *operando* sulfur K-edge X-ray absorption spectroscopy (XAS) and UV−vis spectroscopy to gain the needed complementary information about the mechanism of sulfur reduction together with state and diffusion of polysulfides.[2,36] *Operando* sulfur K-edge XANES spectra were measured during the first discharge of the cell and the corresponding spectra are shown in Figure 5.
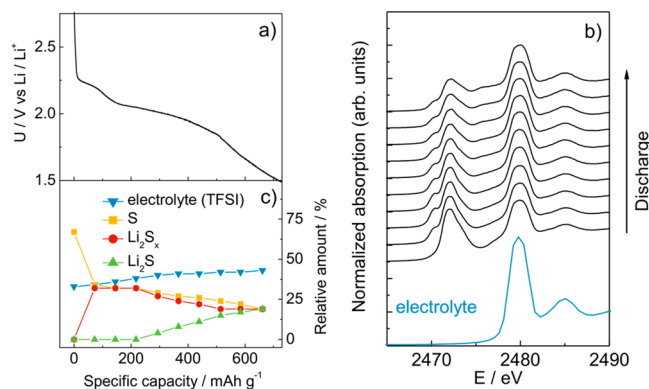

Figure 5. XANES *operando* spectroscopy: (a) electrochemical discharge profile at C/20, (b) sulfur K-edge spectra obtained during the first Li−S cell discharge, (c) relative amounts of each of the four sulfur containing compounds detected during the first discharge.

A principle component analysis (PCA)[44] of the whole set of *operando* XANES spectra (Figure 5b) shows that a linear combination of four different principal components is sufficient to completely describe each XANES spectrum in the series (Figure S8). Candidate components are TFSI, elemental sulfur, lithium polysulfides (Li_2S_x), and lithium sulfide (Li_2S). Using previously recorded reference XANES spectra[2] of sulfur, Li_2S_x, and Li_2S, and a pure electrolyte spectrum measured separately here (diluted with BN), we find the decomposition of all the *operando* XANES spectra to be mathematically reliable and stable even when there is a dominant contribution of a single

one component, as the four reference spectra all are distinctively different. Hence, a linear combination fitting (LCF) analysis allows us to determine the relative amounts of the four sulfur containing compounds in the cathode during the first discharge cycle (Figure 5c).

Clearly, polysulfides are present through the entire discharge process and furthermore monotonously decrease during the discharge along with the elemental sulfur, and their relative amounts are very similar. This behavior we attribute to the limited solubility of polysulfides in the TFEE based electrolyte since a large ratio of polysulfides versus elemental sulfur by the end of the high voltage plateau was previously observed for the "traditional" TEGDME based electrolyte.[2] In both electrolyte systems, the formation of Li_2S starts at the beginning of the low voltage plateau and the precipitation of Li_2S seems to be less influenced by the choice of electrolyte. The coexistence of all three components (sulfur, polysulfides, and Li_2S) can be detected at the end of the discharge process regardless the choice of the electrolyte. Slight increase of electrolyte ratio during discharge process is influenced by pore opening due to sulfur conversion into polysulfides and Li_2S.

To probe the decreased polysulfide diffusion out from the cathode composite into the electrolyte suggested from XANES, *operando* UV−vis spectroscopy was applied (Figure 6). The UV−vis spectra can provide information on the interactions between polysulfides and the electrolyte components as well as the concentrations and chain lengths of the polysulfides.
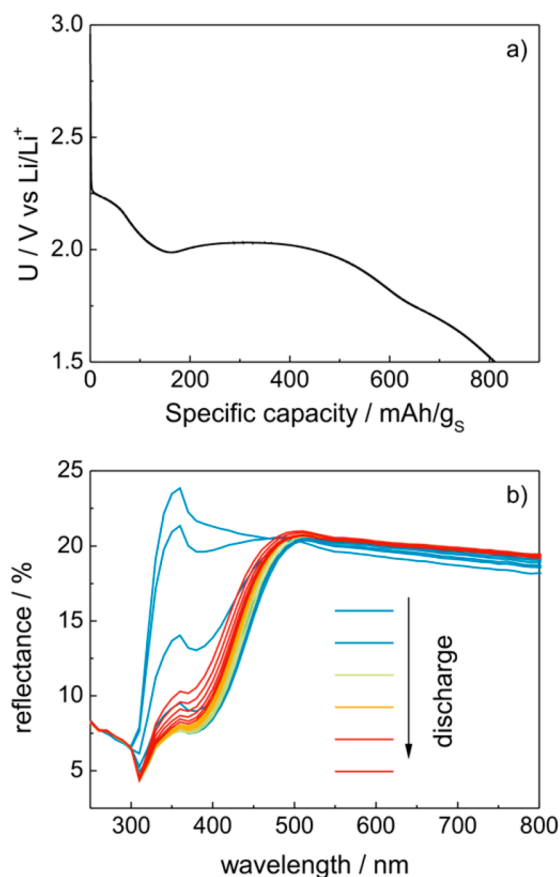
There are clearly polysulfides observed during the high voltage plateau (Figure 6, starting spectra). Because of modified interactions between the polysulfides and the electrolyte components in the fluorinated based electrolytes, as compared to those in a "traditional" electrolyte,[36,37] the UV−vis spectra are all shifted to lower wavelengths, with an absorbance edge at about 400 nm (Figure 6b).

By employing reference spectra, using 2 mM standard solutions of the polysulfides Li_2S_4, Li_2S_6, and Li_2S_8 in the electrolyte, measured in a similar pouch cell setup (Figure S9), we find the long-chain polysulfides to have a maximal absorption at about 440 nm, while shortening the polysulfide chain length shifts the absorption edge to shorter wavelengths. Comparing the derivated *operando* spectra with the standards suggests the presence of mainly long-chain polysulfides; Li_2S_8 and to some extent Li_2S_6 (Figure S10). From a semiquantitative perspective, the UV−vis analysis suggests the concentration of long-chain polysulfides to be a significantly lower in the fluorinated electrolyte than in the "traditional" one where high excess of electrolyte was used.[2] Finally, the UV−vis analysis confirmed the assumption of mainly having long-chain polysulfides dissolved in the electrolyte used in the calculations to be correct.

CONCLUSIONS

A TFEE fluorinated ether based electrolyte results in better capacities and cycling efficiencies in Li−S battery cells as compared to "traditional" electrolytes. High areal capacity with low electrolyte loading can be achieved and significant differences in the length and position of the high voltage plateau were observed.

The altered reaction mechanism was studied with multiple techniques to explain the observed differences in the galvanostatic cell discharge profiles and to reveal whether the conversion involves polysulfide intermediate species, validated by *operando* sulfur K-edge XANES analysis. In addition, UV−vis spectroscopy confirmed a reduced polysulfide solubility and diffusion for the new electrolyte, which arguably reduces the polysulfide shuttling and allows for better electrochemical performance. The molecular level origin for the lower voltage of the first discharge plateau was found to be poor Li^+ ion solvation ability of the fluorinated ethers as analyzed by COSMO-RS computations for several electrolytes. By investigating different ratios of TFEE and DOL, an optimal electrolyte composition was determined and used to construct a high-energy Li−S battery cell with excellent performance characteristics. Overall, this study enables us to claim that a shift of focus from traditional solvents to those with reduced polysulfide (or indeed Li^+) solubility should reduce polysulfide shuttling and be a cheap and easy way for Li−S battery improvement.

ASSOCIATED CONTENT

Ⓢ Supporting Information

The Supporting Information is available free of charge on the ACS Publications website at DOI: 10.1021/acs.chemmater.7b03654.

> GITT experiment; Li metal stability in fluorinated ether electrolyte; high energy Li−S battery cell with different electrolyte loadings; Li^+ solvation investigation with FTIR spectroscopy; XAS experimental details and linear

Figure 6. UV−vis *operando* spectroscopy: (a) electrochemical discharge profile at C/20, (b) spectra obtained during the first Li−S cell discharge.

combination fit; UV−vis spectra of standard polysulfide solutions (PDF)

■ AUTHOR INFORMATION

Corresponding Author
*E-mail: robert.dominko@ki.si.

ORCID
Alen Vizintin: 0000-0003-1876-1396
Robert Dominko: 0000-0002-6673-4459

Notes
The authors declare no competing financial interest.

■ REFERENCES

(1) Rosenman, A.; Markevich, E.; Salitra, G.; Aurbach, D.; Garsuch, A.; Chesneau, F. F. Review on Li-Sulfur Battery Systems: An Integral Perspective. *Adv. Energy Mater.* **2015**, *5*, 1500212−1500233.

(2) Dominko, R.; Patel, M. U. M.; Lapornik, V.; Vizintin, A.; Koželj, M.; Tušar, N.; Arčon, I.; Stievano, L.; Aquilanti, G. Analytical Detection of Polysulfides in the Presence of Adsorption Additives by Operando X-Ray Absorption Spectroscopy. *J. Phys. Chem. C* **2015**, *119*, 19001−19010.

(3) Mikhaylik, Y. V.; Akridge, J. R. Polysulfide Shuttle Study in the Li/S Battery System. *J. Electrochem. Soc.* **2004**, *151*, A1969−A1976.

(4) Diao, Y.; Xie, K.; Xiong, S.; Hong, X. Shuttle Phenomenon − The Irreversible Oxidation Mechanism of Sulfur Active Material in Li−S Battery. *J. Power Sources* **2013**, *235*, 181−186.

(5) Ji, X.; Lee, K. T.; Nazar, L. F. A Highly Ordered Nanostructured Carbon−sulphur Cathode for Lithium−sulphur Batteries. *Nat. Mater.* **2009**, *8*, 500−506.

(6) Rao, M.; Song, X.; Cairns, E. J. Nano-Carbon/sulfur Composite Cathode Materials with Carbon Nanofiber as Electrical Conductor for Advanced Secondary Lithium/sulfur Cells. *J. Power Sources* **2012**, *205*, 474−478.

(7) Guo, J.; Xu, Y.; Wang, C. Sulfur-Impregnated Disordered Carbon Nanotubes Cathode for Lithium-Sulfur Batteries. *Nano Lett.* **2011**, *11*, 4288−4294.

(8) Ahn, W.; Kim, K.-B.; Jung, K.-N.; Shin, K.-H.; Jin, C.-S. Synthesis and Electrochemical Properties of a Sulfur-Multi Walled Carbon Nanotubes Composite as a Cathode Material for Lithium Sulfur Batteries. *J. Power Sources* **2012**, *202*, 394−399.

(9) Wang, H.; Yang, Y.; Liang, Y.; Robinson, J. T.; Li, Y.; Jackson, A.; Cui, Y.; Dai, H. Graphene-Wrapped Sulfur Particles as a Rechargeable Lithium−Sulfur Battery Cathode Material with High Capacity and Cycling Stability. *Nano Lett.* **2011**, *11*, 2644−2647.

(10) Li, N.; Zheng, M.; Lu, H.; Hu, Z.; Shen, C.; Chang, X.; Ji, G.; Cao, J.; Shi, Y. High-Rate Lithium−sulfur Batteries Promoted by Reduced Graphene Oxide Coating. *Chem. Commun.* **2012**, *48*, 4106−4108.

(11) Ji, X.; Evers, S.; Black, R.; Nazar, L. F. Stabilizing Lithium−sulphur Cathodes Using Polysulphide Reservoirs. *Nat. Commun.* **2011**, *2*, 325−331.

(12) Song, M.-S.; Han, S.-C.; Kim, H.-S.; Kim, J.-H.; Kim, K.-T.; Kang, Y.-M.; Ahn, H.-J.; Dou, S. X.; Lee, J.-Y. Effects of Nanosized Adsorbing Material on Electrochemical Properties of Sulfur Cathodes for Li/S Secondary Batteries. *J. Electrochem. Soc.* **2004**, *151*, A791−A795.

(13) Evers, S.; Yim, T.; Nazar, L. F. Understanding the Nature of Absorption/Adsorption in Nanoporous Polysulfide Sorbents for the Li−S Battery. *J. Phys. Chem. C* **2012**, *116*, 19653−19658.

(14) Vizintin, A.; Patel, M. U. M.; Genorio, B.; Dominko, R. Effective Separation of Lithium Anode and Sulfur Cathode in Lithium-Sulfur Batteries. *ChemElectroChem* **2014**, *1*, 1040−1045.

(15) Su, Y.-S.; Manthiram, A. Lithium−sulphur Batteries with a Microporous Carbon Paper as a Bifunctional Interlayer. *Nat. Commun.* **2012**, *3*, 1166−1171.

(16) Lee, Y. M.; Choi, N.-S.; Park, J. H.; Park, J.-K. Electrochemical Performance of Lithium/sulfur Batteries with Protected Li Anodes. *J. Power Sources* **2003**, *119*, 964−972.

(17) Cuisinier, M.; Cabelguen, P.-E.; Adams, B. D.; Garsuch, A.; Balasubramanian, M.; Nazar, L. F. Unique Behaviour of Nonsolvents for Polysulphides in Lithium−sulphur Batteries. *Energy Environ. Sci.* **2014**, *7*, 2697−2705.

(18) Lee, C. W.; Pang, Q.; Ha, S.; Cheng, L.; Han, S. D.; Zavadil, K. R.; Gallagher, K. G.; Nazar, L. F.; Balasubramanian, M. Directing the Lithium-Sulfur Reaction Pathway via Sparingly Solvating Electrolytes for High Energy Density Batteries. *ACS Cent. Sci.* **2017**, *3*, 605−613.

(19) Gu, S.; Qian, R.; Jin, J.; Wang, Q.; Guo, J.; Zhang, S.; Zhuo, S.; Wen, Z. Suppressing the Dissolution of Polysulfides with Cosolvent Fluorinated Diether towards High-Performance Lithium Sulfur Batteries. *Phys. Chem. Chem. Phys.* **2016**, *18*, 29293−29299.

(20) Cheng, L.; Curtiss, L. A.; Zavadil, K. R.; Gewirth, A. A.; Shao, Y.; Gallagher, K. G. Sparingly Solvating Electrolytes for High Energy Density Lithium−Sulfur Batteries. *ACS Energy Lett.* **2016**, *1*, 503−509.

(21) Azimi, N.; Xue, Z.; Bloom, I.; Gordin, M. L.; Wang, D.; Daniel, T.; Takoudis, C.; Zhang, Z. Understanding the Effect of a Fluorinated Ether on the Performance of Lithium−Sulfur Batteries. *ACS Appl. Mater. Interfaces* **2015**, *7*, 9169−9177.

(22) Patel, M. U. M.; Arčon, I.; Aquilanti, G.; Stievano, L.; Mali, G.; Dominko, R. X-Ray Absorption near-Edge Structure and Nuclear Magnetic Resonance Study of the Lithium-Sulfur Battery and Its Components. *ChemPhysChem* **2014**, *15*, 894−904.

(23) Klamt, A. Conductor-like Screening Model for Real Solvents: A New Approach to the Quantitative Calculation of Solvation Phenomena. *J. Phys. Chem.* **1995**, *99*, 2224−2235.

(24) Klamt, A.; Eckert, F. COSMO-RS: A Novel and Efficient Method for the a Priori Prediction of Thermophysical Data of Liquids. *Fluid Phase Equilib.* **2000**, *172*, 43−72.

(25) Klamt, A. The COSMO and COSMO-RS Solvation Models. *Wiley Interdiscip. Rev. Comput. Mol. Sci.* **2011**, *1*, 699−709.

(26) Klamt, A. COSMO-RS for Aqueous Solvation and Interfaces. *Fluid Phase Equilib.* **2016**, *407*, 152−158.

(27) Ahlrichs, R.; Bär, M.; Häser, M.; Horn, H.; Kölmel, C. Electronic Structure Calculations on Workstation Computers: The Program System Turbomole. *Chem. Phys. Lett.* **1989**, *162*, 165−169.

(28) TURBOMOLE, Version 7.1; TURBOMOLE GmbH: Germany, 2016.

(29) Becke, A. D. Density-Functional Exchange-Energy Approximation with Correct Asymptotic Behavior. *Phys. Rev. A: At., Mol., Opt. Phys.* **1988**, *38*, 3098−3100.

(30) Perdew, J. P. Density-Functional Approximation for the Correlation Energy of the Inhomogeneous Electron Gas. *Phys. Rev. B: Condens. Matter Mater. Phys.* **1986**, *33*, 8822−8824.

(31) Schäfer, A.; Huber, C.; Ahlrichs, R. Fully Optimized Contracted Gaussian Basis Sets of Triple Zeta Valence Quality for Atoms Li to Kr. *J. Chem. Phys.* **1994**, *100*, 5829−5835.

(32) Eckert, F.; Klamt, A. COSMOthermX Version C30_1701; COSMOlogic GmbH & Co. KG: Leverkusen, Germany, 2016.

(33) Azimi, N.; Weng, W.; Takoudis, C.; Zhang, Z. Improved Performance of Lithium−sulfur Battery with Fluorinated Electrolyte. *Electrochem. Commun.* **2013**, *37*, 96−99.

(34) Jeschke, S.; Johansson, P. Predicting the Solubility of Sulfur: A COSMO-RS-Based Approach to Investigate Electrolytes for Li-S Batteries. *Chem. - Eur. J.* **2017**, *23*, 9130−9136.

(35) Aquilanti, G.; Giorgetti, M.; Dominko, R.; Stievano, L.; Arčon, I.; Novello, N.; Olivi, L. *Operando* Characterization of Batteries Using X-Ray Absorption Spectroscopy: Advances at the Beamline XAFS at Synchrotron Elettra. *J. Phys. D: Appl. Phys.* **2017**, *50*, 74001.

(36) Patel, M. U. M.; Demir-Cakan, R.; Morcrette, M.; Tarascon, J. M.; Gaberscek, M.; Dominko, R. Li-S Battery Analyzed by UV/vis in Operando Mode. *ChemSusChem* **2013**, *6*, 1177−1181.

(37) Patel, M. U. M.; Dominko, R. Application of in Operando UV/Vis Spectroscopy in Lithium-Sulfur Batteries. *ChemSusChem* **2014**, *7*, 2167−2175.

(38) Zhang, T.; Marinescu, M.; O'Neill, L.; Wild, M.; Offer, G. Modeling the Voltage Loss Mechanisms in Lithium-Sulfur Cells: The Importance of Electrolyte Resistance and Precipitation Kinetics. *Phys. Chem. Chem. Phys.* **2015**, *17*, 22581−22586.

(39) Loschen, C.; Klamt, A. Solubility Prediction, Solvate and Cocrystal Screening as Tools for Rational Crystal Engineering. *J. Pharm. Pharmacol.* **2015**, *67*, 803−811.

(40) Chen, J.; Han, K. S.; Henderson, W. A.; Lau, K. C.; Vijayakumar, M.; Dzwiniel, T.; Pan, H.; Curtiss, L. A.; Xiao, J.; Mueller, K. T.; et al. Restricting the Solubility of Polysulfides in Li-S Batteries Via Electrolyte Salt Selection. *Adv. Energy Mater.* **2016**, *6*, 1600160−1600165.

(41) MacDonald, S. M.; Opallo, M.; Klamt, A.; Eckert, F.; Marken, F. Probing Carboxylate Gibbs Transfer Energies via Liquid|liquid Transfer at Triple Phase Boundary Electrodes: Ion-Transfer Voltammetry versus COSMO-RS Predictions. *Phys. Chem. Chem. Phys.* **2008**, *10*, 3925.

(42) Soustelle, M. Solvents and Solvation. In *Ionic and Electrochemical Equilibria*; John Wiley & Sons, Inc.: Hoboken, NJ, 2016; pp 31−59.

(43) Isele-Holder, R. E.; Rabideau, B. D.; Ismail, A. E. Definition and Computation of Intermolecular Contact in Liquids Using Additively Weighted Voronoi Tessellation. *J. Phys. Chem. A* **2012**, *116*, 4657−4666.

(44) Ravel, B.; Newville, M. ATHENA, ARTEMIS, HEPHAESTUS: Data Analysis for X-Ray Absorption Spectroscopy Using IFEFFIT. *J. Synchrotron Radiat.* **2005**, *12*, 537−541.